Title	Electromagnetic design of a new hybrid-excited flux-switching machine for fault-tolerant operations
Author(s)	Lin, F; Chau, KT; Liu, C; Qiu, C; Liu, CH
Citation	The 41st Annual Conference of the IEEE Industrial Electronics Society (IECON 2015), Yokohama, Japan, 9-12 November 2015. In Conference Proceedings, 2015, p. 2521-2525
Issued Date	2015
URL	http://hdl.handle.net/10722/232289
Rights	Annual Conference of Industrial Electronics Society Proceedings. Copyright © IEEE.; ©2015 IEEE. Personal use of this material is permitted. Permission from IEEE must be obtained for all other uses, in any current or future media, including reprinting/republishing this material for advertising or promotional purposes, creating new collective works, for resale or redistribution to servers or lists, or reuse of any copyrighted component of this work in other works.; This work is licensed under a Creative Commons Attribution-NonCommercial-NoDerivatives 4.0 International License.

Electromagnetic Design of a New Hybrid-Excited Flux-Switching Machine for Fault-Tolerant Operations

Fei Lin, K. T. Chau, Chunhua Liu, and Chun Qiu
Department of Electrical and Electronic Engineering, the University of Hong Kong, Hong Kong, China
Shenzhen Institute of Research and Innovation, the University of Hong Kong, Hong Kong

Chunhua Liu
School of Energy and Environment,
City University of Hong Kong, Hong Kong, China
chualiu@eee.hku.hk

***Abstract*— In this paper, a new hybrid-excited flux-switching (HEFS) machine is proposed with the outer-rotor configuration, which possesses the distinct feature of fault-tolerant operation. Comparing with the conventional permanent-magnet (PM) machine, it combines merits of flux control, high mechanical integrity, and low-cost. Furthermore, its fault-tolerant feature ensures its continuous operation in the event of winding faults. Hence, a new 12/10-pole HEFS machine is designed and implemented in this paper. By using time-stepping finite element method, open circuit (OC) fault and short circuit (SC) faults on the armature winding are investigated in the proposed machine for the fault-tolerant operation. The phase-current reconfiguration and flux control are applied for the remediation of the OC fault, while the SC faults is remedied by the phase-current reconfiguration merely. Both approaches demonstrate their good performances for the fault-tolerant operation.**

Keywords—hybrid-excited, flux-switching machine, fault-tolerant operation, finite-element-method (FEM).

I. INTRODUCTION

FAUT-TOLERANT capability has been paid increasing attention in recent years on the machine design, which ensures the machine's continuous operation in the event of abnormal connection of windings, such as open circuit (OC) fault, short circuit (SC) fault, etc. [1]-[4]. Lately, the hybrid-excited flux-switching (HEFS) machine attracts a great attention for its merits of flexible flux control and wide-speed constant-power operation [5]-[8]. It utilizes both DC field winding and permanent-magnets (PMs) as excitation sources. With these unique features, this kind of machines can be further operated at faulty situations with acceptable performances. However, few literatures investigate both OC fault and SC fault together for this kind of machine (only OC fault [9]-[11]).

Hence, this paper aims to investigate the fault-tolerant operation of a new HEFS machine, including remedial operations for the OC fault and SC fault. In terms of the OC fault, the remaining healthy phases can be reconfigured to achieve the remedial operation, which is called the phase-current reconfiguration [5], [12]. It can also be remedied by simply utilizing the field excitation boosting to achieve the flux-control [5], [13]. For the SC fault, phase-current reconfiguration is utilized to remedy the shorted-phase loss. Hence, by using time-stepping finite element method (TS-FEM), these two types of winding faults are analyzed, compared, and verified by applying the proposed approaches.

II. MACHINE DESIGN

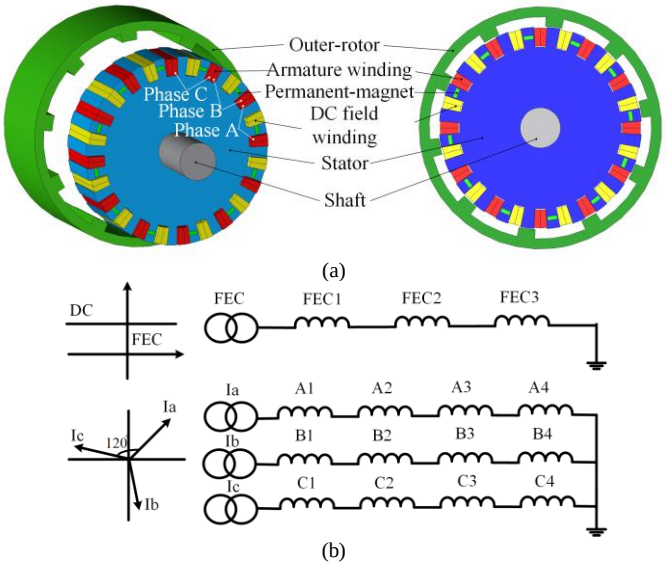

Fig. 1. (a) Exploded structure of the proposed HEFS machine. (b) Circuit representations of the field excitation coil three-phase armature windings

Fig. 1(a) shows the 3D exploded diagram of the proposed 12/10-pole HEFS machine. The outer rotor is merely a single piece iron with neither PMs and coils, which makes the structure more robust. The stator contains 12 slots armature coils, 12 slots field excitation coils (FECs), and 12 PMs. It can be found that four groups of armature windings are distributed in 12 slots periodically, which are supplied with sinusoidal three-phase currents. The alternate 12 slots are twined with FECs that are excited with a constant DC current source.

Fig. 1(b) shows the circuit design for the field excitation coil and three-phase armature windings. The field excitation coil is excited by a constant DC current source. The armature

TABLE I
KEY DATA OF THE PROPOSED MACHINE

Item	Value
Rotor outside diameter	480.0 mm
Rotor inside diameter	401.2 mm
Stator outside diameter	400.0 mm
Stator inside diameter	80.0 mm
Air-gap length	0.60 mm
Stack length	200.0mm
Number of rotor poles	10
Number of stator poles	24
Number of excitation poles	12
Number of AC phases	3
Rotational speed	1000 rpm

windings are supplied by a three-phase AC power. It is noted that all the windings are divided into multiple sections for a better performance on the fault-tolerant operation.

The relationship of the number of rotor poles, the stator poles and the filed winding poles pairs are shown as follows:

$$N_s = m \times N_c \tag{1}$$
$$N_r = N_s \pm 2 \tag{2}$$

where N_r is the number of rotor poles, N_s the number of stator poles, m the number of phases, N_c the number of coils per phase [14]-[16]. In this machine design, the parameters are selected as m = 3, N_c = 4. Hence, it has N_r = 10, N_s =12. Hence, the machine is designed with 24 stator poles and 10 rotor poles. The corresponding key data for the proposed machine is listed in Table I.

III. PRINCIPLE OF FAULT-TOLERANT OPERATION

In this paper, fault-tolerant operations focus on three types of winding faults, namely, one-phase OC fault, half-phase SC fault, and one-phase SC fault. Two approaches are proposed for the fault-tolerant operation, namely, phase-current reconfiguration and flux control. The operational principles of these two approaches are described as follows.

A. Phase-Current Reconfiguration

Phase-current reconfiguration aims to reconstruct the magnitudes and phase angles of the phase currents to keep the magnetomotive force (MMF) constant after fault occurs.

Under normal condition: The sinusoidal three-phase currents are expressed as [17]:

$$\begin{cases} i_a = I\cos\theta \\ i_b = I\cos(\theta + 2\pi/3) \\ i_c = I\cos(\theta - 2\pi/3) \end{cases} \tag{3}$$

The corresponding phasor diagram is shown in Fig. 2(a). It can be found that the three-phase current phasor is 120° apart in space from each other with the same magnitude. The rotating MMF generated by the three-phase currents can be

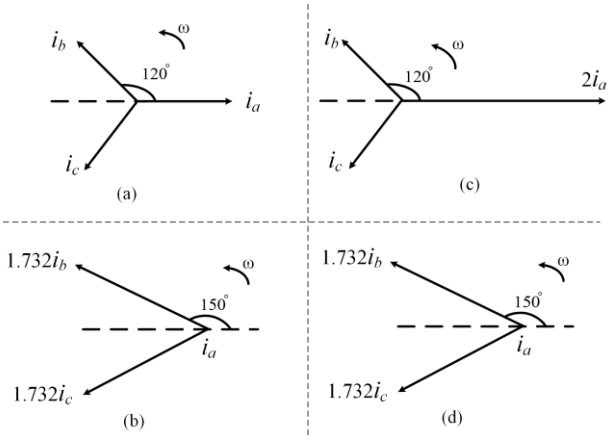

Fig. 2. Current-phasor diagrams under different conditions. (a) Normal condition. (b) One-phase OC fault. (c) Half-phase SC fault. (d) One-phase SC fault.

expressed as [18]-[19]:

$$MMF = MMF_a + MMF_b + MMF_c = Ni_a + aNi_b + a^2Ni_c \tag{4}$$

where N is the number of turns of each phase, a = $1\angle$-120°. By substituting (1) into (2), the rotating MMF can be deduced as:

$$MMF = 3NI_2(\cos\theta + j\sin\theta)/2 = 3NI_2e^{j\theta}/2 \tag{5}$$

Under open circuit fault: Assume phase A is open-circuited, the new current of phase A turns to be zero. Hence, the rotating MMF generated by the remaining two phases can be expressed as:

$$\begin{aligned} MMF &= MMF_a' + MMF_b' + MMF_c' = Ni_a' + aNi_b' + a^2Ni_c' \\ &= aNi_b' + a^2Ni_c' \end{aligned} \tag{6}$$

As described for the phase-current reconfiguration, the rotating MMF can be kept constant by reconfiguring the amplitudes of angles of the phase currents. By equating (5) and (6), the remedial three-phase currents are deduced as (7). The corresponding phasor diagram is shown in Fig. 2(b). By comparing with the phasor diagram in Fig. 2(a), it can be found that amplitudes of the remedial phase A and phase B are increased by $\sqrt{3}$, while their phase angles are lagged by 30 degrees.

$$\begin{cases} i_a' = 0 \\ i_b' = \sqrt{3}I\cos(\theta + 5\pi/6) \\ i_c' = \sqrt{3}I\cos(\theta - 5\pi/6) \end{cases} \tag{7}$$

Under short circuit condition: Assume *m* turns of phase A

are short circuited $(0 < m < N)$, then *(N-m)* turns of phase A are under operation. By introducing the definition of the rotating MMF, the new rotating MMF generated by the three-phase currents can be expressed as:

$$\begin{aligned} MMF &= MMF_a^{''} + MMF_b^{''} + MMF_c^{''} \\ &= (N-m)i_a^{''} + aNi_b^{''} + a^2 Ni_c^{''} \end{aligned} \tag{8}$$

The remedial three-phase currents are assumed as (9). In order to keep the rotating MMF constant, by equating (8), (9) and (5), the relationship among I_a^{max}, I_b^{max}, I_c^{max}, N, and M is assumed as (10).

$$\begin{cases} i_a^{''} = I_a^{max} \cos\theta \\ i_b^{''} = I_b^{max} \cos(\theta + 2\pi/3) \\ i_c^{''} = I_c^{max} \cos(\theta - 2\pi/3) \end{cases} \tag{9}$$

$$((N-m)/N) I_a^{max} = I_b^{max} = I_c^{max} \tag{10}$$

Hence, when *m = N/2*, phase A is half-phase short-circuited. The remedial three-phase currents are deduced as (11). The corresponding phasor diagram is shown in Fig. 2(c). It is found that the magnitude of phase A is twice than the magnitudes of the other two phases.

$$\begin{cases} i_a^{''} = 2I\cos\theta \\ i_b^{''} = I\cos(\theta + 2\pi/3) \\ i_c^{''} = I\cos(\theta - 2\pi/3) \end{cases} \tag{9}$$

When $N = M$, the entire phase A is short-circuited. Under this condition, the entire phase A can be disconnected and disabled, which can be regarded as the open-circuit fault. Thus, its phasor diagram showing in Fig. 2(d) is the same as the one-phase OC fault. The corresponding remedial operation can refer to the OC fault section.

B. Flux Control

Flux control aims to boost the electromagnetic torque by strengthening the air gap density, which can be achieved by adjusting the field excitation.

The electromagnetic torque T_{FC} under flux control can be given by [20]-[22]:

$$\begin{aligned} T_{FC} &= T_f + T_{pm} + T_r \\ &= i\,d\Phi_f/d\theta + i\,d\Phi_{pm}/d\theta + (i^2/2)dL/d\theta \end{aligned} \tag{11}$$

where θ is the rotor position, i is the armature phase current, T_f, T_{pm}, and T_r are the DC field torque, PM torque, and reluctance torque respectively, Φ_f, Φ_{pm}, and Φ_r are their corresponding flux linkages.

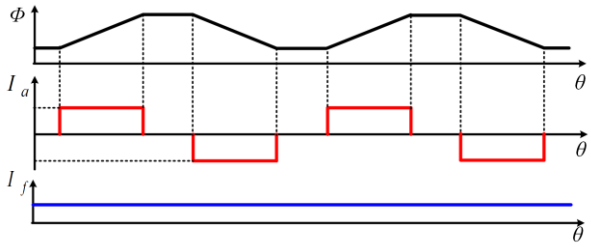

Fig. 3. Theoretical operating waveform

Hence, it can be found in (11) that the electromagnetic torque is affected by the flux linkages and armature phase current. The corresponding theoretical operating waveform is presented in Fig. 3 [23]-[26]. The armature phase current I_a is a bipolar rectangular current with a conduction angle of 120°. The field excitation source I_f is supplied by a constant DC current. When the flux linkage Φ is increasing, a positive I_a is applied to produce a positive torque. When Φ is decreasing, a negative I_a is applied to produce a positive torque [27]-[30]. Hence, for the flux control strengthening, it is possible to boost the field excitation to enhance the air gap flux density. Note that flux control operation is merely tested for the one-phase OC fault in this study.

IV. FAULT-TOLERANT PERFORMANCE

By using time-stepping finite-element-method (TS-FEM), the fault-tolerant performances of the proposed machine are presented. In order to achieve fault tolerant operations under the phase-current reconfiguration mode and flux control, the sinusoidal and rectangular currents are fed into the armature windings, respectively.

Fig. 4 shows the output torques and three-phase current waveforms with two types of input phase currents under normal operation. As expected, the input current waveforms are sinusoidal and rectangular with 180° and 120° conduction angles in Fig. 4(a) and Fig. 4(b), respectively. And it can be found that their average torque outputs are nearly the same, around 27 Nm.

For the one-phase OC fault, remedial phase-current reconfiguration and remedial flux control are applied. As shown in Fig. 5(a) and Fig. 5(b), with the phase-current reconfiguration, the output torque increases from 17.9 Nm to 26.9 Nm after remediation. While the torque ripple presents a distinct improvement from 136.1% to 42.5%. With the remedial flux control in Fig. 5(c) and Fig. 5(d), the output torque almost maintains the normal operation after remediation, while its torque ripple is still large with a slight improvement.

For the half-phase SC fault and one-phase SC fault, remedial phase-current reconfiguration is conducted. Fig. 6(a) and Fig. 6(b) are the performances of half-phase SC. It can be found

that output torque is enhanced from 21.6 Nm to 27.3 Nm by double the magnitude of phase A, while its ripple decreases from 105.1% to 87.3%. For the one-phase SC fault in Fig. 6(c), the faulty phase is disconnected and treated as one-phase OC fault. Hence the remedial result shown in Fig. 6(d) is similar to the one in Fig. 5(b). The key data of the torque performances are collected in Table I.

Table I summarizes the key data of the fault-tolerant operations with OC fault and SC faults. The average torque outputs under one-phase OC fault, half-phase SC fault, and one-phase SC fault are 17.9 Nm, 21.6 Nm, and 12.3 Nm respectively. It can be found that all the fault-tolerant operations successfully boost the average torque outputs to the normal level after faults occur, which are around 27 Nm. The torque ripples are around 70% under phase-current reconfiguration and 110% under flux-control, which indicates the flux-control operation has a higher torque ripple than the phase-current configuration.

TABLE I
KEY DATA OF TORQUE PERFORMANCES

Operating Mode	Average Torque	Torque Ripple
Normal	27.4 Nm	39.1 %
One-phase OC fault	17.9 Nm	136.1 %
Remedial Phase-current reconfiguration	26.9 Nm	42.5 %
Remedial Flux control	27.2 Nm	115.6 %
Half-phase SC fault	21.6 Nm	105.1 %
Remedial Phase-current reconfiguration	27.3 Nm	70.3 %
One-phase SC fault	12.3 Nm	350.1 %
Remedial Phase-current reconfiguration	27.1 Nm	42.8 %

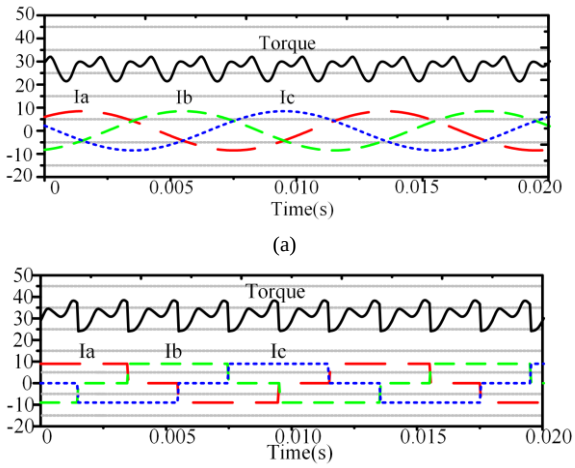

Fig. 4. Output torques and three-phase current waveforms under normal operation. (a) Sinusoidal three-phase currents. (b) Rectangle three-phase currents.

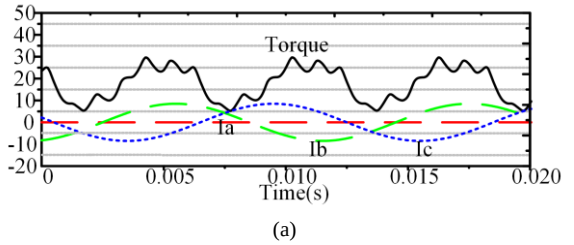

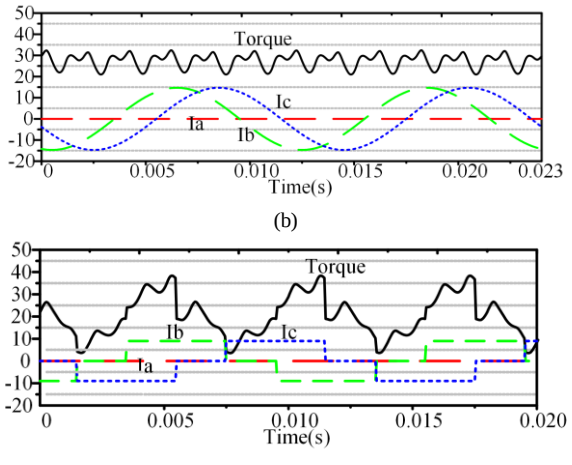

Fig. 5. Fault-tolerant operations for OC fault. (a) One-phase OC fault. (b) Remedial phase-current reconfiguration. (c) Remedial flux-control.

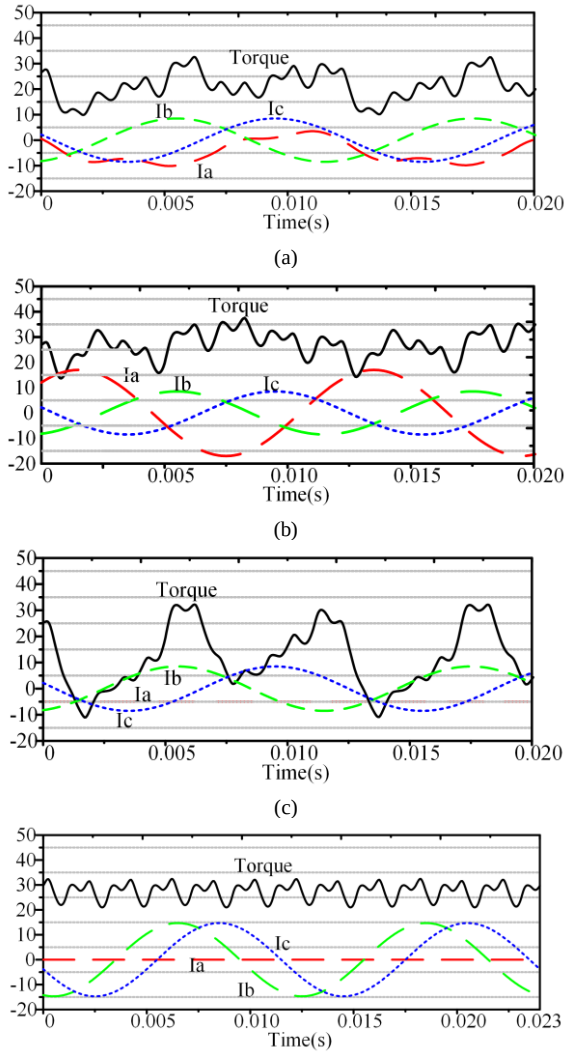

Fig. 6. Fault-tolerant operations for SC fault. (a) Half-phase SC fault. (b) Remedial phase-current reconfiguration for half-phase SC fault. (c) One-phase SC fault. (d) Remedial phase-current reconfiguration for one-phase SC fault.

V. CONCLUSION

In this paper, a new HEFS machine with outer-rotor structure is proposed and implemented. By using TS-FEM, two fault-tolerant approaches are tested and analyzed for OC fault and SC fault, namely, phase-current reconfiguration and flux control. The simulation results demonstrate that the proposed approaches are able to maintain the normal output torque after faults occur. The flux control shows a lager torque ripple output than the phase-current reconfiguration, but its operation principle is simpler.

ACKNOWLEDGMENT

This work was supported and funded by the grant of Basic Research Program (Project Code: JCYJ20120831142942515), Science, Technology and Innovation Commission of Shenzhen municipality (SZSTI), China.

REFERENCES

[1] C. Liu, K.T. Chau, J.Z. Jiang, L. Jian , "Design of a new outer-rotor permanent magnet hybrid machine for wind power generation", *IEEE Trans. Magn.*, vol. 44, no. 6, pp. 1494-1497, 2008.

[2] F. Lin, K.T. Chau, C.C. Chan, C. Liu, "Fault diagnosis of power components in electric vehicles", *Journal of Asian Electric Vehicles*, vol. 11, no. 2, 2013.

[3] B. Akin, C. Seungdeog, U. Orguner, and H.A. Toliyat, "A simple real-time fault signature monitoring tool for motor-drive-embedded fault diagnosis systems," *IEEE Trans. Ind. Electron.*, vol. 58, no. 5, pp. 1990-2001, May 2011.

[4] S. Nandi, H.A. Toliyat, and X.D. Li, "Condition monitoring and fault diagnosis of electrical motors-a review," *IEEE Trans.Energy Convers.*, vol. 20, no. 4, pp. 719-729, Dec. 2005.

[5] C. Liu, K.T. Chau, W. Li, "Comparison of fault-tolerant operation for permanent-magnet hybrid brushless motor drive", *IEEE Tran. Magn.*, vol. 46, no. 6, pp. 1378-1381, 2010.

[6] Y. Tang, J.J.H. Paulides, T.E. Motoasca, E.A. Lomonova, "Flux-switching machine with DC excitation", *IEEE Trans. on Magn.*, vol. 48, no. 11, pp. 3583-3586, Nov. 2012.

[7] C. Liu, K.T. Chau, J.Z. Jiang and S. Niu, "Comparison of stator-permanent-magnet brushless machines," *IEEE Trans. on Magn.*, vol. 44, no. 11, pp. 4405-4408, Nov. 2008.

[8] W.X. Zhao, M. Cheng, K.T. Chau, and C.C. Chan, "Control and operation of fault-tolerant flux-switching permanent-magnet motor drive with second harmonic current injection," *IET Electric Power Applications.*, vol. 6, no. 9, pp. 707-715, Nov. 2012.

[9] W. Ding, Y. Liu, Y. Hu, "Performance evaluation of a fault-tolerant decoupled dual-channel switched reluctance motor diver under open-circuit," *IET Electric Power Applications*, vol. 8, no. 4, pp. 117-130, 2014.

[10] D. Rivelino, D.U. Campos-Delgado, G. Bossio, E. Barcenas, J.E. Hernandez-Diez, L.F. Lugo-Cordero, "Fault diagnosis scheme for open-circuit faults in field-oriented control induction motor drives," *IET Power Electronics*, vol. 6, no. 5, pp. 869-877, 2013.

[11] S. Khwan-on, L. De lillo, L. Empringham, P. Wheeler, C. Gerada, "Fault-tolerant, matrix converter, permanent magnet synchronous motor drive for open-circuit failures," *IET Electric Power Applications*, vol. 5, no. 8, pp. 654-667, 2011.

[12] M.D.S. Aderiano, "Induction motor fault diagnostic and monitoring methods," Master, Electrical and Computer Enginnering, Marquette University, Milwaukee, Wisconsin, 2006.

[13] Z. Wang and K.T. Chau, "Design, analysis and experimentation of chaotic permanent magnet DC motor drives for electric compaction," IEEE Transactions on Circuits and Systems II: Express Briefs, vol. 56, no. 3, pp. 245-249, Mar. 2009.

[14] C. Liu, K.T. Chau, J.Z. Jiang, L. Jian , "Design of a new outer-rotor permanent magnet hybrid machine for wind power generation", *IEEE Trans. Magn.*, vol. 44, no. 6, pp. 1494-1497, 2008.

[15] K.T. Chau, Y.B. Li, J.Z. Jiang and C. Liu, "Design and analysis of a stator-doubly-fed doubly-salient permanent-magnet machine for automotive engines," *IEEE Trans. on Magn.*, vol. 42, no. 10, pp. 3470-3472, Oct. 2006.

[16] K.T. Chau and W. Li, "Overview of electric machines for electric and hybrid vehicles," *(Invited Paper) International Journal of Vehicle Design*, vol. 64, no. 1, pp. 46-71, 2014.

[17] C. Liu and K.T. Chau, "Electromagnetic design and analysis of double-rotor flux-modulated permanent-magnet machines," *Progress In Electromagnetics Research*, vol. 131, pp. 81-97, 2012.

[18] G.J. Offer, V. Yufit, D.A. Howey, B. Wu, and N.P. Brandon, "Module design and fault diagnosis in electric vehicle batteries," *Journal of Power Sources*, vol. 206, pp. 383-392, May 2012.

[19] S. Niu, S.L. Ho, W.N. Fu, K.T. Chau, and F. Lin, "A feasibility study on a new brushless and gearless contra-rotating permanent magnet wind power generator." *Journal of Applied Physics*, vol. 115, no. 17, pp. 1-3, May 2014.

[20] Y. Gong, K. T. Chau, J. Z. Jiang, C. Yu, and W. Li, "Design of doubly salient permanent magnet motors with minimum torque ripple," *IEEE Trans. Magn.*, vol. 45, no. 10, pp. 4704–4707, Oct. 2009.

[21] F. Li, K.T. Chau, C. Liu and C. Qiu, "New approach for pole-changing with dual-memory machine," IEEE Transactions on Applied Superconductivity, vol. 24, no. 3, paper no. 501504, pp. 1-4, June 2014.

[22] H.A. Toliyat, S. Nandi, and S. Choi, *Electric Machines: Modeling, Condition Monitoring, and Fault Diagnosis*: Taylor & Francis Group, 2012.

[23] C. Liu, K.T. Chau, and Z. Zhang, "Novel design of double-stator single-rotor magnetic-geared machines" *IEEE Trans. on Magn.*, vol. 48, no. 11, pp. 4180-4183, Nov. 2012.

[24] B. Akin, C. Seungdeog, U. Orguner, and H.A. Toliyat, "A simple real-time fault signature monitoring tool for motor-drive-embedded fault diagnosis systems," *IEEE Trans. Ind. Electron.*, vol. 58, no. 5, pp. 1990-2001, May 2011.

[25] M. Chen, K.T. Chau, W. Li, C. Liu and C. Qiu, "Design and analysis of a new magnetic gear with multiple gear ratios," *IEEE Trans. on Applied Supercon.*, vol. 24, no. 3, pp. 1-4, June 2014.

[26] C. Liu, K.T. Chau, and C. Qiu, "Design and analysis of a new magnetic-geared memory machine," *IEEE Trans. on Applied Supercon.*, vol. 24, no. 3, pp. 1-5, June 2014.

[27] W Li, K.T. Chau, C. Liu and C. Qiu, "Design and analysis of a flux-controllable linear variable reluctance machine," *IEEE Trans. on Applied Supercon.*, vol. 24, no. 3, , pp. 1-4, June 2014.

[28] C.H.T. Lee, K.T. Chau, C. Liu and C. Qiu, "Design and analysis of a new multitoothed magnetless doubly-salient machine," IEEE Transactions on Applied Superconductivity, *IEEE Trans. on Applied Supercon.*, vol. 24, no. 3, pp. 1-4, June 2014.

[29] Y. Du, M. Cheng, K.T. Chau, X. Liu, F. Xiao, W. Zhao, K. Shi, and L. Mo, "Comparison of linear primary permanent magnet vernier machine and linear vernier hybrid machine," *IEEE Trans. on Magn.*, vol. 50, no. 11, pp. 1-4, Nov. 2014.

[30] X. Li, K.T. Chau, and M. Cheng, "Analysis, design and experimental verification of a field-modulated permanent-magnet machine for direct-drive wind turbines," *IET Electric Power Applications*, vol. 9, no. 2, pp. 150-159, Feb. 2015.